# 18-DEGREE-OF-FREEDOM CONTROLLER DESIGN FOR THE ST7 DISTURBANCE REDUCTION SYSTEM

## F. L. Markley,* P. G. Maghami,* M. B. Houghton,* and O. C. Hsu*

The Space Technology 7 experiment will perform an on-orbit system-level validation of a Disturbance Reduction System employing gravitational reference sensors and micronewton colloidal thrusters to maintain a spacecraft's position with respect to free-floating test masses in the gravitational reference sensors to less than 10 nm/√Hz over the frequency range 1 to 30 mHz. This paper presents the design and analysis of the control system that closes the loop between the gravitational reference sensors and the micronewton thrusters while incorporating star tracker data at low frequencies. The effects of disturbances and actuation and measurement noise are evaluated in a eighteen-degree-of-freedom model.

## INTRODUCTION

NASA's New Millennium Program has selected the Disturbance Reduction System (DRS) flight validation experiment for the Space Technology 7 (ST7) mission.[1] New Millennium missions are intended to validate advanced technologies that have not flown in space in order to reduce the risk of their infusion in future NASA Space Science missions. ST7, managed by the Jet Propulsion Laboratory and scheduled to fly on the European Space Agency's SMART-2 spacecraft in 2006, incorporates two specific DRS technologies. A highly sensitive Gravitational Reference Sensor (GRS), provided by Stanford University, measures the position and attitude of a spacecraft with respect to an internal free-floating test mass; and a set of micronewton colloidal thrusters, provided by the Busek Company, provides control forces. The ST7 DRS is designed to maintain the spacecraft's position, with respect to the GRS free-floating test mass, to less than 10 nm/√Hz, over ST7's science measurement frequency range from 1 to 30 mHz. The DRS instrument package consists of two gravitational reference sensors, two sets of four micronewton thrusters each for position and attitude control, an interferometer to measure the distance between the two test masses, and associated electronics, as shown in Figure 1.

This paper presents the overall design and analysis process of the spacecraft controller being developed at NASA's Goddard Space Flight Center to close the loop between the GRS and the micronewton colloidal thrusters. The essential dynamics of the ST7-DRS are captured in a simulation including eighteen rigid-body dynamic degrees of freedom: three translations and three rotations for the spacecraft and for each test mass. Actuation and measurement noise and disturbance sources acting on the spacecraft and test masses are modeled. The ST7 DRS comprises three control systems: the attitude control system (ACS) to maintain a sun-pointing attitude; the drag free control to center the spacecraft about the test masses; and the test mass suspension control. This paper summarizes the control design and analysis of the ST7-DRS 18-DOF model, and is an extension of previous analyses employing a 7-DOF planar model of ST-7.[2,3]

*Mission Engineering and Systems Analysis Division, NASA Goddard Space Flight Center, Greenbelt, MD 20771
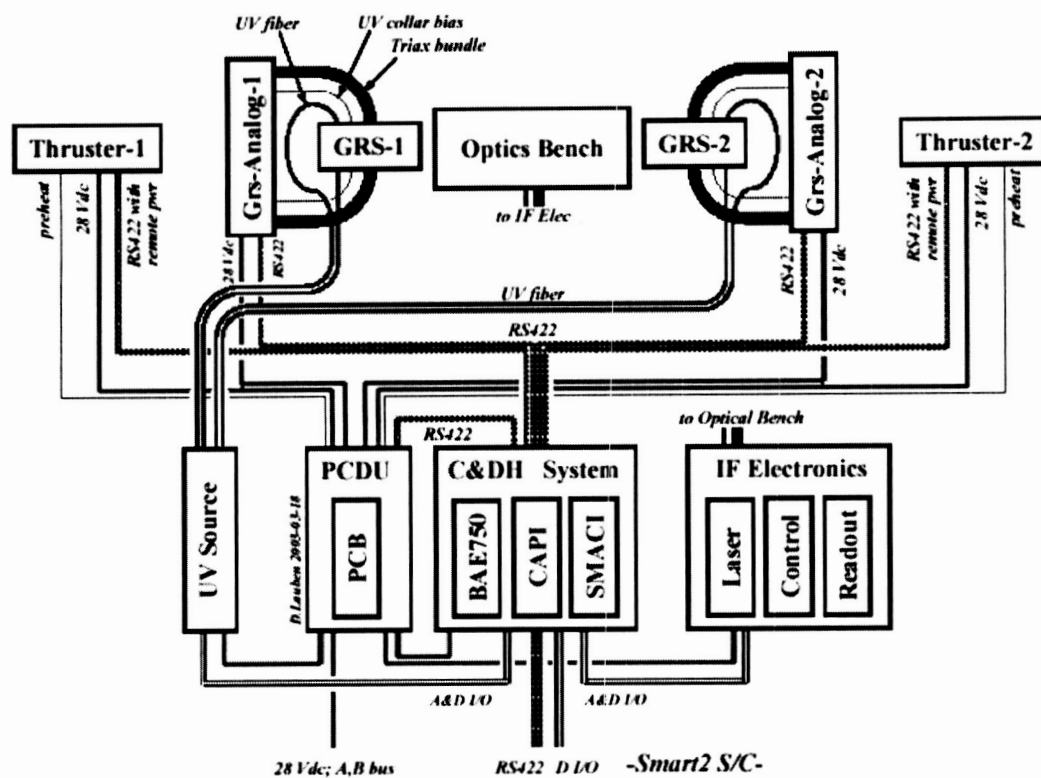
**Figure 1. DRS Instrument Schematic**

## MODEL DESCRIPTION

The location and the orientation of the two test masses in the model can be arbitrarily assigned. The nominal position vectors for the two test masses and their respective housings are chosen as $R_1 = [-0.1 \quad 0.05 \quad 0.3]$ m and $R_2 = [0.1 \quad 0.05 \quad 0.3]$ m, which means that the sensitive axis is along the $x$-axis of the spacecraft. The mass of the spacecraft and the test masses are assumed to be 300 kg and 1.25 kg, respectively.

Two clusters, each containing four thrusters, are located on the $\pm x$ faces to provide thrust capability for attitude and drag-free control. Figure 2 is perspective drawing of one of the thruster clusters. The larger protruding cylinders are the four thrusters that emit positively charged particles to provide the thrust. The smaller cylinders are the neutralizers that emit electrons to maintain the charge neutrality of the spacecraft. The assembly contains the thruster power supplies and electronics, and enough propellant to fire each of the four thrusters at maximum thrust for the length of the ST7 mission. Each thruster provides a force that is continuously variable from 2 $\mu$N to 20 $\mu$N in 0.1 $\mu$N increments. The clusters are mounted on the spacecraft as shown in Figure 3.
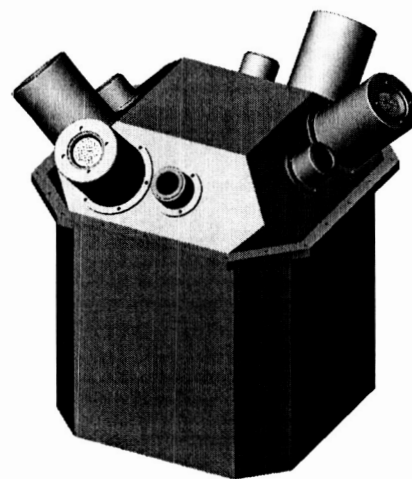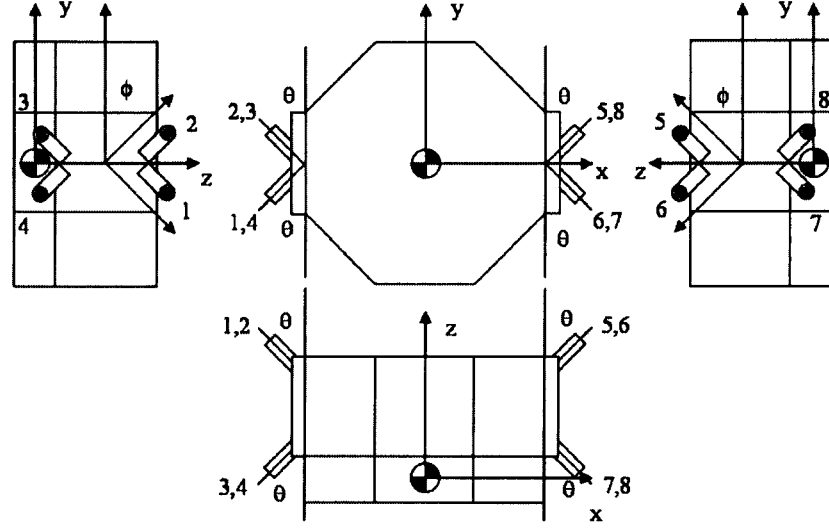


**Figure 2 Cluster of Four Thrusters**

**Figure 3 Positioning of the Thrusters on the SMART-2 Spacecraft**

The force $\mathbf{F}$ (in $\mu$N) and torque $\mathbf{T}$ (in $\mu$N-m) on the spacecraft are related to the individual thrusts (in $\mu$N), arrayed in a eight-dimensional vector $\tau$, by

$$\begin{bmatrix} \mathbf{F} \\ \mathbf{T} \end{bmatrix} = H_{authority}\tau = \begin{bmatrix} 0.707 & 0.707 & 0.707 & 0.707 & -0.707 & -0.707 & -0.707 & -0.707 \\ 0.500 & -0.500 & -0.500 & 0.500 & -0.500 & 0.500 & 0.500 & -0.500 \\ -0.500 & -0.500 & 0.500 & 0.500 & -0.500 & -0.500 & 0.500 & 0.500 \\ -0.235 & 0.235 & 0.165 & -0.165 & 0.235 & -0.235 & -0.165 & 0.165 \\ 0.083 & 0.083 & 0.483 & 0.483 & -0.083 & -0.083 & -0.483 & -0.483 \\ -0.250 & 0.250 & 0.250 & -0.250 & -0.250 & 0.250 & 0.250 & -0.250 \end{bmatrix}\tau. \tag{1}$$

The matrix $H_{authority}$ has rank six, as is required to control six degrees of freedom. Its null space is spanned by the vectors $[1\ 0\ 1\ 0\ 1\ 0\ 1\ 0]^T$ and $[0\ 1\ 0\ 1\ 0\ 1\ 0\ 1]^T$. In order to generate a desired force and thrust, the individual thruster commands are computed using the pseudoinverse of the authority matrix

$$\tau_{cmnd} = H_{dist}\begin{bmatrix} \mathbf{F}_{desired} \\ \mathbf{T}_{desired} \end{bmatrix} = \begin{bmatrix} 0.427 & -1.164 & -0.25 & -3.536 & -0.625 & -0.5 \\ 0.427 & 1.164 & -0.25 & 3.536 & -0.625 & 0.5 \\ -0.073 & -1.164 & 0.25 & -3.536 & 0.625 & 0.5 \\ -0.073 & 1.164 & 0.25 & 3.536 & 0.625 & -0.5 \\ -0.427 & 1.164 & -0.25 & 3.536 & 0.625 & -0.5 \\ -0.427 & -1.164 & -0.25 & -3.536 & 0.625 & 0.5 \\ 0.073 & 1.164 & 0.25 & 3.536 & -0.625 & 0.5 \\ 0.073 & -1.164 & 0.25 & -3.536 & -0.625 & -0.5 \end{bmatrix}\begin{bmatrix} \mathbf{F}_{desired} \\ \mathbf{T}_{desired} \end{bmatrix}. \tag{2}$$

Since a thruster cannot develop negative thrust, the thrusters must all be biased to a positive value so that adding $\tau_{cmnd}$ results in an overall command between 2 $\mu$N and 20 $\mu$N for each thruster. The biases must also counteract the steady force due to solar radiation pressure of 20 $\mu$N in the $-z$ direction. A convenient choice for the bias is

$$\tau_{bias} = [6\ 6\ 16\ 16\ 6\ 6\ 16\ 16]^T\ \mu N, \tag{3}$$

since this gives a force of 20 $\mu$N in the $+z$ direction with no torque, and allows the components of $\tau_{cmnd}$ to vary between $\pm4$ $\mu$N. It is possible to change the thruster mounting angles to achieve equal biases on all the thrusters. This has the advantage of limiting the relative thrust variations around the bias value, but does

result in some reduction of command authority. Equation (2) clearly shows that the command authority is weakest for $x$ axis torque commands, which is already obvious from the thruster configuration shown in Figure (3). It is an imnportant feature of the system design that the $x$ axis is parallel to the line between the proof masses, since this is the axis requiring the least torque authority.

Two disturbances are included in this model. The first is the nominal solar radiation pressure and its variation. The Sun exposed face of the spacecraft corresponds to the $z$ direction. The angle of the incident rays of the sun to the surface normal may be arbitrarily assigned, but is assumed to be zero for the current analysis. The frequency spectrum used for solar radiation flux variations given in Figure 4 represents a conservative assessment of measured variations.[4,5] This plot indicates a constant spectrum at the frequencies below 0.1 mHz, followed by a $1/f$ roll off. This spectrum also includes the so-called 5-minute acoustic oscillation (at 3.5 mHz), and levels off at frequencies above 10 mHz. The second disturbance source modeled was the acceleration noise on the test mass. A number of sources contribute to this acceleration noise, including magnetic and Lorentz forces, thermal disturbances, cosmic ray impacts, etc.[2] The spectral density function for the test mass acceleration noise is assumed to have: $1/f^2$ rolloff at frequency range of 0.01-0.1 mHz, $1/f$ rolloff at frequency range of 0.1-1 mHz, and constant spectral density $3 \times 10^{-14}$ m/s$^2$/√Hz at frequencies above 1 mHz. The linear filter approximation to this frequency spectrum shown in Figure 5 meets or exceeds all disturbance levels. This acceleration noise was applied to both test masses in all directions in this analysis. White-noise models were used to capture thruster noise, electrostatic suspension force noise, star tracker noise, and the capacitive sensing noise (used to measure the positions of the test masses relative to the spacecraft). The intensity levels are captured in Table 1.

## CONTROLLER DESIGN AND ANALYSIS

A top-level block diagram of the system dynamics is shown in Figure 6. The drag-free controller controls the position of the spacecraft to establish free-fall motion of one of the test masses. Either test mass can be chosen as the drag-free reference, but the analysis in this paper chooses test mass 1 The spacecraft attitude control orients the spacecraft in the low frequency band (DC and near DC) using the star tracker data, and centers the spacecraft about the other test mass (test mass 2 in this paper) in the transverse ($y$ and $z$) directions in the measurement band. Both test masses are effectively freely falling in the ST7 science measurement band from 1 to 30 mHz. The 18-DOF model also includes the electrostatic suspension control of the test masses. The controllers were designed using a classical control approach, but the 18-DOF system is a MIMO system by virtue of the cross coupling between the relative test mass positions and the attitude of the spacecraft. The four control loops were implemented within a MATLAB-based model of the system. This MATLAB model serves as the design and analysis tool for the 18-DOF Model.
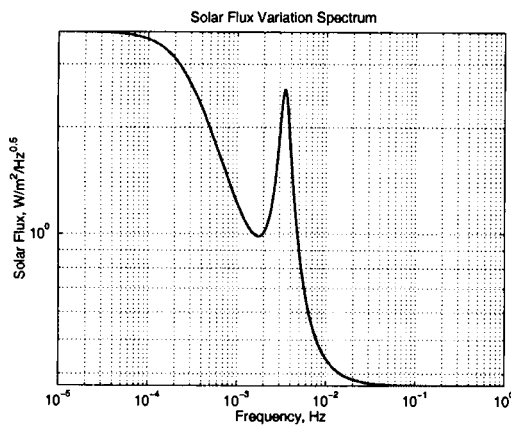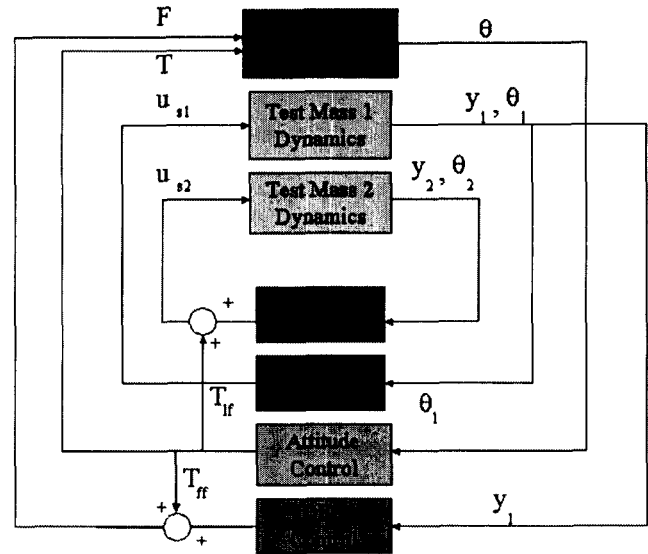


**Figure 4 Root Power Spectrum of the Solar Radiation Flux Variations**
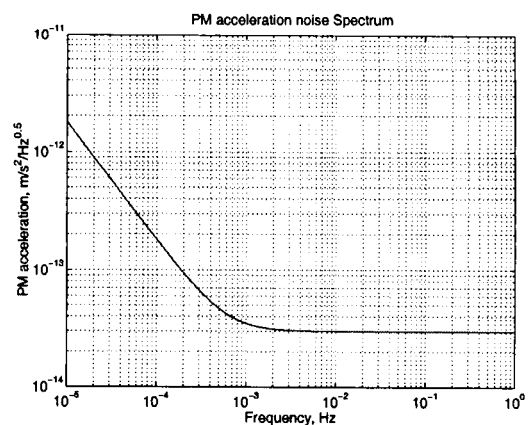
**Figure 5 Root Power Spectrum for the Test Mass Acceleration Noise**

**Table 1**
**Actuation and Sensing Noise Intensities**

| Noise Source | Intensity |
|---|---|
| Thrusters | 0.1 $\mu$N/$\sqrt{}$Hz |
| Suspension Force | 2e-14 N/$\sqrt{}$Hz |
| Star Tracker | 20 arcsec/$\sqrt{}$Hz |
| Capacitive Sensing | 3 nm/$\sqrt{}$Hz |

**Figure 6 Block Diagram of Drag-Free Control Strategy**

The performance requirements for drag-free control system (DCS) are summarized as:

- The drag-free control DCS shall keep the spacecraft pointed to within $\pm 5°$ of the Sun.

- The DCS shall control the spacecraft position with respect to the drag-free reference test mass to better than 10 nm/$\sqrt{}$Hz over the frequency range of 1 mHz to 30 mHz.

- The DCS shall control the spacecraft attitude to maintain the position of the test mass (not the drag-free reference) with respect to its housing to better than 10 nm/$\sqrt{}$Hz over the frequency range of 1 mHz to 30 mHz, in the transverse directions.

- The DCS shall limit spacecraft acceleration to keep force levels on both test masses within the GRS electrostatic suspension limits.

- The DCS commands to the individual thrusters shall be in the range of 2 $\mu$N to 20 $\mu$N.

All sensor measurements are updated at 10 Hz sampling with the exception of the star tracker signal, which is updated at 1 Hz sampling. There are four control loops, controlling the attitude and position of the spacecraft as well as the relative attitude and position of the two test masses. The attitude control loop is responsible for maintaining the Sun pointing within the specified requirements in the low frequency regime (DC and near DC). However, it is also responsible for maintaining test mass 2 drag-free, in transverse directions, in the science band (1 mHz-30 mHz). It is a 7-input/3-output controller, which uses the three attitude errors (obtained from the star tracker measurement) and the relative position errors of the test masses in the transverse directions to compute the required spacecraft torque commands.

$$\mathbf{T}(s) = K_{al}(s)\,\boldsymbol{\theta}(s) + K_{ah}(s)\begin{bmatrix} y_1(s) \\ z_1(s) \\ y_2(s) \\ z_2(s) \end{bmatrix} \qquad (4)$$

Here, $K_{al}(s)$ denotes the low-bandwidth part of the attitude control designed to maintain the attitude of the spacecraft. It is a position-integral-derivative (PID) controller with an appropriate attenuation filter, resulting in a fifth-order controller (crossover frequency at 0.01 mHz). $K_{ah}(s)$ represents the part of the attitude controller responsible for centering the spacecraft about test mass (not drag-free reference) in the transverse directions. The relative position error of the test masses in the transverse direction are used to compute the required rotation (in GRS frame) of the GRS package about the drag-free reference test mass. The required rotation command is then transformed into S/C frame and is used as input to a SISO-based controller to regulate the S/C attitude in the science band. To obtain a pure rotation about the first test mass, feedforward translation commands are generated and issued to the drag-free controller. This controller is also designed based on the classical approach, and is a series combination of a lead-lag filter, position-derivative (PD) filter, and a roll-off filter, resulting in a seventh-order controller. The second control loop is the drag-free controller, which controls the position of the spacecraft to establish drag-free motion of test mass 1. The drag-free control loops were designed using a classical control approach, resulting in crossover frequencies between 0.055 and 0.06 Hz. As mentioned earlier, a feedforward compensation is implemented in the drag-free control to allow for pure rotation of the GRS about one test mass and to reduce the attitude/translation couplings. The controller is given by

$$\mathbf{u}_{DFC}(s) = K_{DFC}(s) \begin{bmatrix} x_1(s) \\ y_1(s) \\ z_1(s) \end{bmatrix} + \mathbf{p}_1 \times [H\ \mathbf{T}(s)], \tag{5}$$

where $\mathbf{p}_1$ is the position of test mass 1 relative to the system center of mass and $H$ is a matrix depending on spacecraft inertia properties.

The suspension control system, which maintains the relative attitude of both test masses (with respect to their respective housings) and the relative position of the test mass (non-reference) around DC, is being developed by Stanford University. Preliminary 3-D control designs and noise models have been provided by Stanford. However, these controllers had to be modified to accommodate stability margin requirements of the ST7/DRS controls. The position control, in transverse directions is a low bandwidth controller to provide disturbance rejection at DC and near DC. In the current design, there is no feedforward commanding of the gravitational sensors. This simplifies the design process as well as clearly delineates the requirements.

**Stability Margins**

The block diagram of the system in Figure 6 shows 15 scalar outputs and 15 inputs. The 15 measurements used by the control system are the spacecraft attitude error from the star tracker, relative position and attitude of the drag-free reference test mass, and the relative position and attitude of the other test mass. The 15 control inputs are the thruster force and torque commands in the spacecraft frame, and the suspension control torque commands for the drag-free reference test mass, followed by the suspension control force and torque commands for the other test mass. The controller for each loop was designed independently using classical design techniques. However, the 18-DOF Model, by the virtue of cross coupling between relative test mass positions and the attitude of the spacecraft, represents a MIMO system. Hence, the loop gains for each input and output channel (while the remaining channels are closed) must be analyzed for proper stability margins. Each control loop was required to have: 6 dB gain margin and 35° phase margin, which are ample considering that the effects of zero-order hold and computational and transport delays are already included in the analysis. The margins for 18 of the 30 channels are shown in Table 2. The other 12 channels, the three components of the sensed attitude of the two test masses relative to their housings and the three components of the suspension torque commands for each test mass, all have gain margins of 22 dB and phase margins of 51°.

**Table 2 Gain and Phase Margins**

| Channel | Gain Margin (dB) | Phase Margin (deg) |
|---|---|---|
| Star tracker output - $x$ | 18 | 55 |
| Star tracker output - $y$ | 10 | 39 |
| Star tracker output - $z$ | 10 | 37 |
| Test mass 1 position relative to housing - $x$ | 6 | 36 |
| Test mass 1 position relative to housing - $y$ | 6 | 35 |
| Test mass 1 position relative to housing - $z$ | 6 | 35 |
| Test mass 2 position relative to housing - $x$ | 27 | 48 |
| Test mass 2 position relative to housing - y | 9 | 39 |
| Test mass 2 position relative to housing - z | 9 | 37 |
| Thrust torque command - $x$ | 18 | 54 |
| Thrust torque command - y | 9 | 39 |
| Thrust torque command - $z$ | 9 | 39 |
| Thrust force command - $x$ | 6 | 36 |
| Thrust force command - $y$ | 6 | 35 |
| Thrust force command - $z$ | 6 | 35 |
| Test mass 2 suspension force command - $x$ | 27 | 48 |
| Test mass 2 suspension force command - $y$ | 9 | 58 |
| Test mass 2 suspension force command - $z$ | 8 | 53 |

## System Performance

Both time-domain and frequency-domain analyses were performed, but only the frequency domain results are presented here, since the system requirements are stated in terms of power spectral densities. The root power spectral density plots in Figures 7-24 show the contributions of the various disturbance sources. The contribution of each disturbance category represents the root sum squared (RSS) values for that category; for example, the thruster noise plot is the RSS contribution of the noise from all eight thrusters.

Figures 7-12 illustrate the root power spectral densities of the relative positions of both test masses with respect to their respective housings. These relative positions must obey a PSD requirement of 10 nm/√Hz for both test masses in the science band, which is the most stringent requirement on the ST7 drag-free control. This required performance level is along the top of the plot in Figures 7-9, and is indicated by a horizontal dashed line in Figures 10-12. The plots show that the system satisfies these stringent requirements, with spectra being mainly dominated by the thruster noise and measurement noise. It is possible to reduce the peak PSDs in the vicinity of 30 mHz at the expense of requiring more high-frequency thruster activity; the current design is a near-optimal compromise of these requirements. The root power spectral density of the relative position of test mass 1 is also below 10 nm/√Hz at all frequencies outside the measurement band, but the root power spectral density of the relative position of test mass 2 exceeds this level at DC and near DC frequencies. This is unavoidable with the ST7 GRS orientations, since it is impossible for both proof masses to be drag-free simultaneously at all frequencies.

Figures 13-18 illustrate the spectra for the spacecraft thruster force and torque commands. The RSS levels are mainly dominated by the thruster noise in the measurement band and at lower frequencies. Capacitive sensing noise makes the largest contribution to the variations in the thrust force and $y$ and $z$ axis thrust torque commands above the measurement band, especially in the 100-200 mHz range. The $x$ axis thrust torque command falls off much more rapidly than the other thrust commands in and above the measurement band, reflecting the much looser requirements on $x$ axis rotations. As mentioned above, this is fortunate, since the thruster layout results in minimal torque authority about this axis. The root spectrum for individual thruster commands were computed but are not presented in this paper. They are very similar in

both magnitude and frequency dependence to the thruster force commands shown in Figures 13-15, showing significant thruster activity in the 100-200 mHz frequency range.

The root power spectral densities of the spacecraft attitude pointing errors are shown in Figures 19-21. Although, the requirement on the spacecraft pointing is fairly coarse, these figures indicate a fairly tight steady-state pointing performance. They are almost completely dominated by thruster noise.

The root power spectral densities of the suspension forces for test mass 2 illustrated in Figures 22-24 are within acceptable range of accelerations on the test masses. They are dominated by thruster noise up to 0.1 Hz and by capacitive sensing noise above that frequency. The root power spectral densities of the suspension forces for test mass 1 are identically zero in this analysis, since no suspension forces are apppied to the drag-free test mass. The test mass relative attitude errors and suspension torques were computed but are not presented in this paper. The suspension attitude controllers used in the analysis are place holders; the actual controllers are being designed by the Stanford University GRS team.

## CONCLUSIONS

Our analyses show that all the requirements for the ST7-DRS control system are met in the eighteen-degree-of-freedom model. These requirements include establishing drag-free motion of the test masses in the science band as well as spacecraft attitude control. The spacecraft position relative to the primary test mass is maintained within the required precise limits, and successful spacecraft attitude control is accomplished by combining low frequency data from a star tracker and high frequency data from the transverse position of the second test mass. Rapidly rolling off the electrostatic suspension forces on the second test mass between DC and the measurement frequency band provides adequate suspension while maintaining its drag-free state within the frequency range of interest.

## REFERENCES

[1] Keiser, G. M., Buchman, S., Byer, R. L., Folkner, W. M., Hruby, V., and Gamero-Castaño, M., "Disturbance Reduction System for Testing Technology for Drag-Free Operation," SPIE Paper 4856-02, Astronomical Telescopes and Instrumentation Conference, Waikoloa, Hawaii, USA, August 2002.

[2] Maghami, P. G., Markley, F. L., Dennehy, C. J., Houghton, M. B., and Folkner, W. M., "Controller Design for the ST7 Disturbance Reduction System," 5th International Conference on Guidance, Navigation, and Control Systems, Frascati, Italy, Oct. 22–25, 2002

[3] Maghami, P. G., Markley, F. L., Houghton, M. B., and Dennehy, C. J., "Design and Analysis of the ST7 Disturbance Reduction System (DRS) Spacecraft Controller," AAS 03-165, AAS Guidance and Control Conference, Breckenridge, CO, Feb. 5–9, 2003

[4] Final Technical Report of the (Phase A) Study of the Laser Interferometer Space Antenna (Dornier Satellintensysteme GmbH – Matra Marconi Space – Alenia Aerospzio) ESTEC Contract no. 13631/99/NL/MS, Report No. LI-RP-DS-009, April 2000

[5] Pap, J. et. al., "Variation in Total Solar and Spectral Irradiance as Measured by the VIRGO Experiment on SOHO", *Adv. Space Res.*, 24:215-224, 1999.
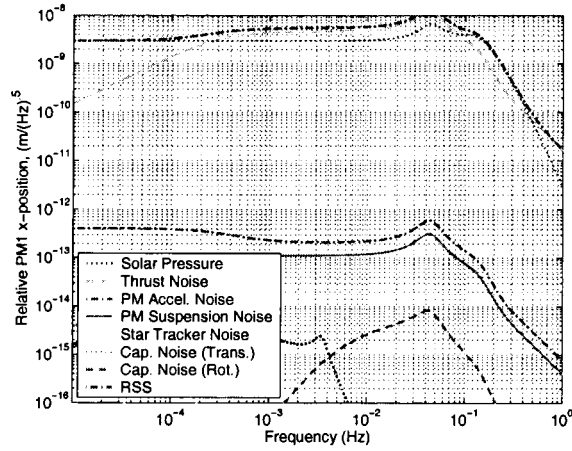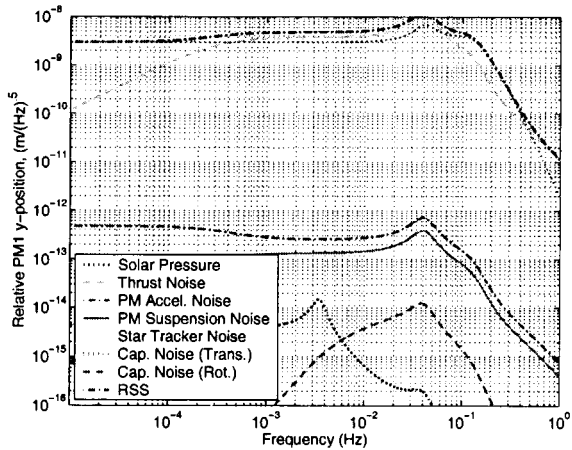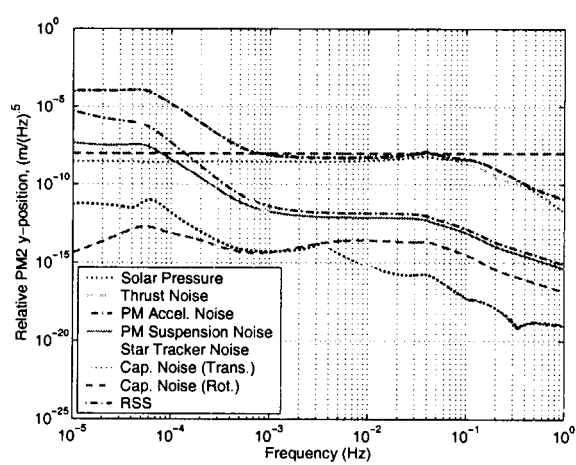
**Figure 7 Root Power Spectrum of the Relative Position of Test Mass 1: *x*-Direction**
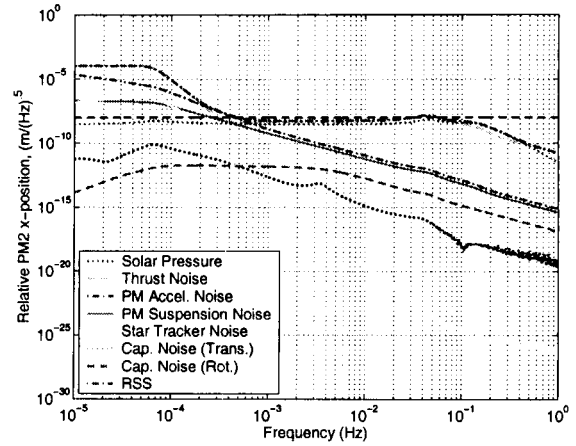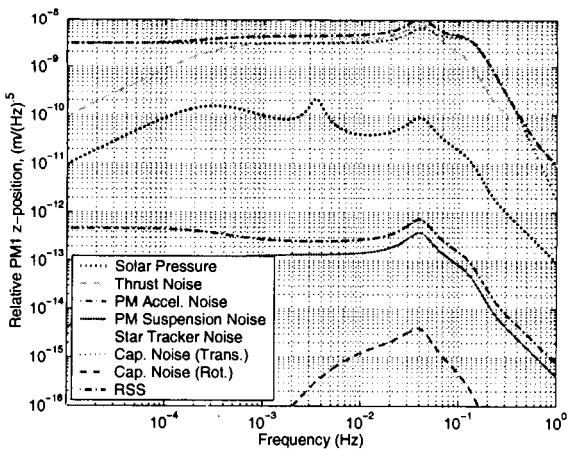


**Figure 10 Root Power Spectrum of the Relative Position of Test Mass 2: *x*-Direction**
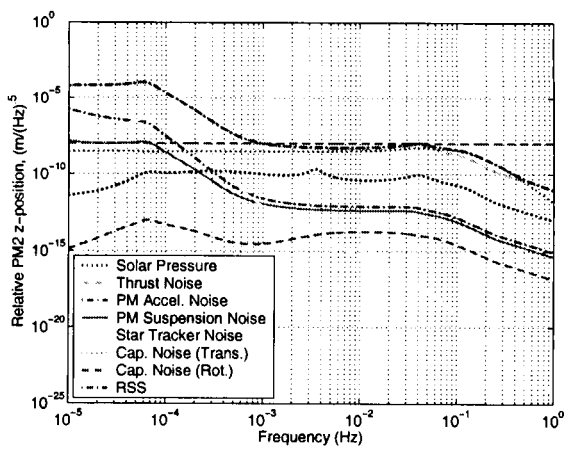


**Figure 8 Root Power Spectrum of the Relative Position of Test Mass 1: *y*-Direction**
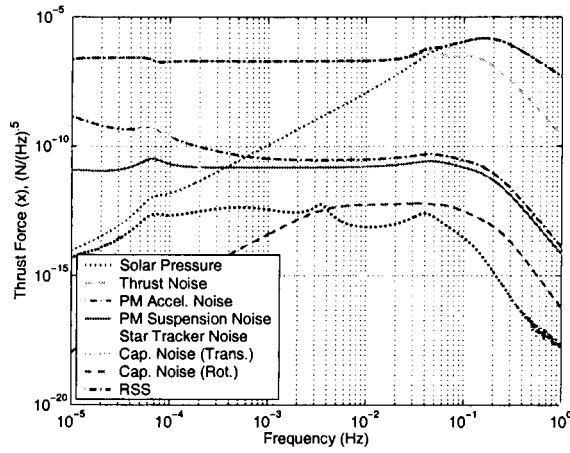


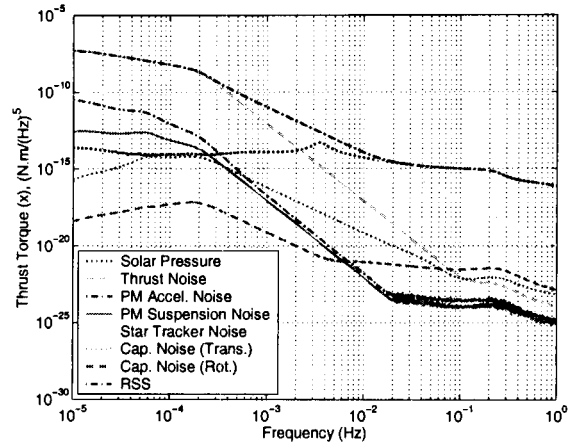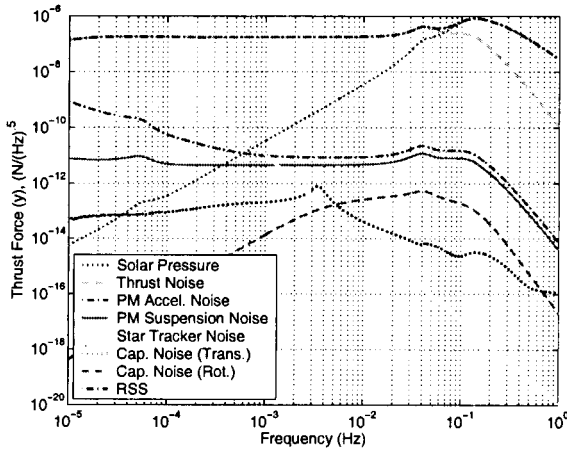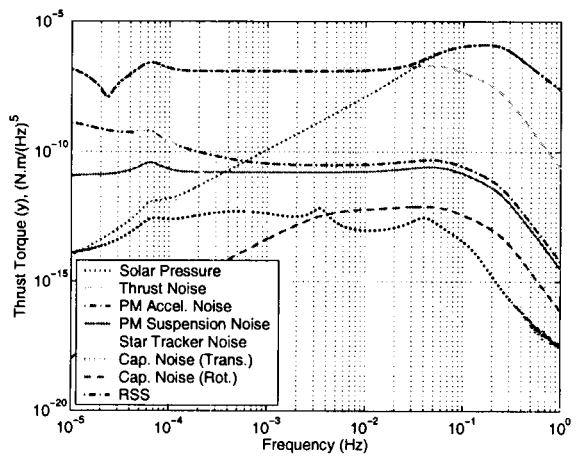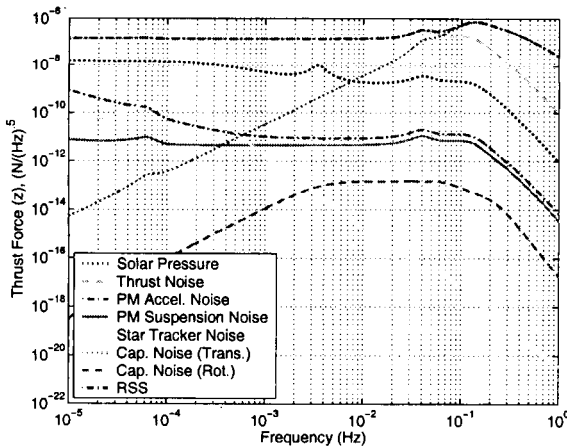**Figure 11 Root Power Spectrum of the Relative Position of Test Mass 2: *y*-Direction**



**Figure 9 Root Power Spectrum of the Relative Position of Test Mass 1: *z*-Direction**



**Figure 12 Root Power Spectrum of the Relative Position of Test Mass 2: *z*-Direction**

**Figure 13 Root Power Spectrum of the Thrust Force: *x*-Direction**



**Figure 16 Root Power Spectrum of the Thrust Torque: *x*-Direction**



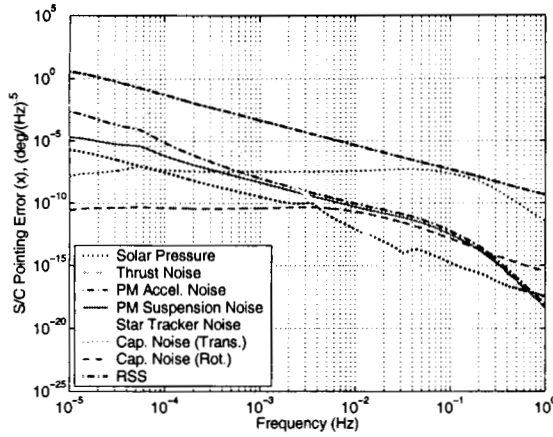**Figure 14 Root Power Spectrum of the Thrust Force: *y*-Direction**



**Figure 17 Root Power Spectrum of the Thrust Torque: *y*-Direction**
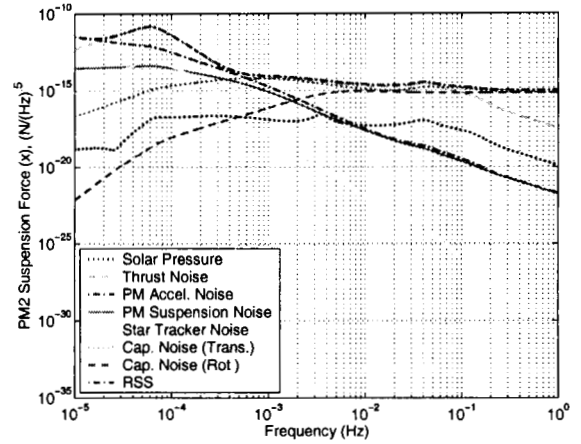


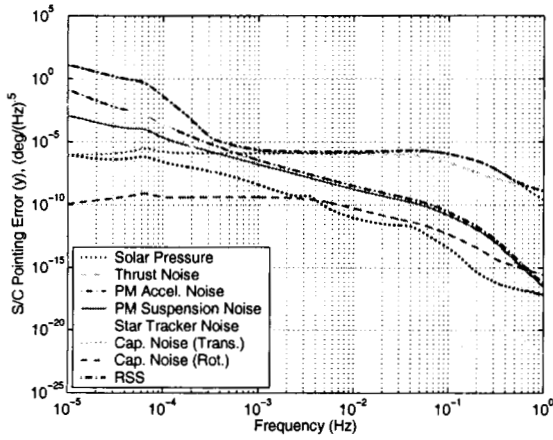**Figure 15 Root Power Spectrum of the Thrust Force: *z*-Direction**
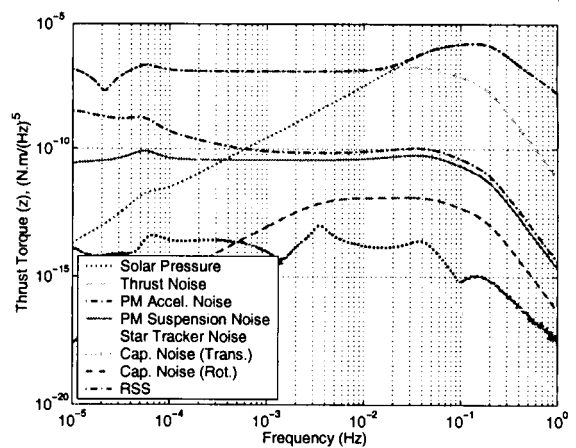


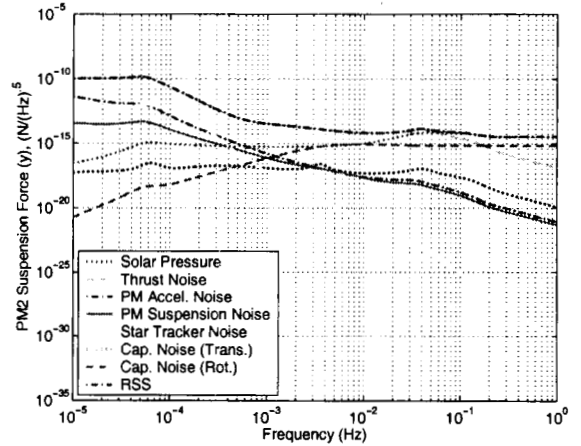**Figure 18 Root Power Spectrum of the Thrust Torque: *z*-Direction**

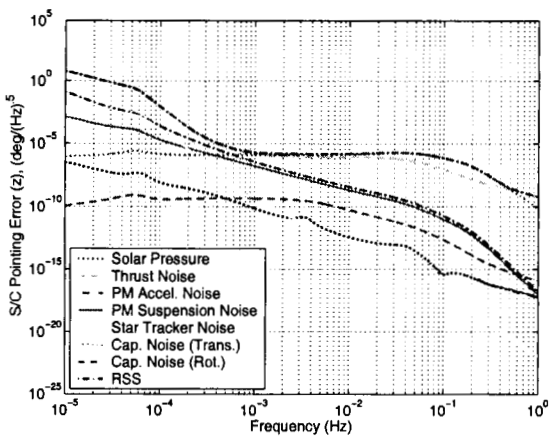**Figure 19 Root Power Spectrum of the Spacecraft Attitude Error: *x*-Direction**



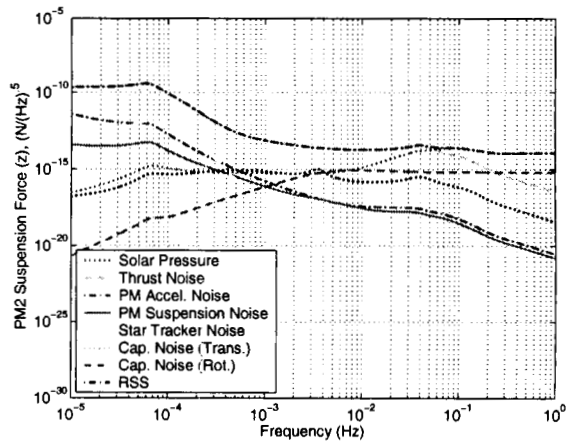**Figure 22 Root Power Spectrum of the Test Mass 2 Suspension Force - *x***



**Figure 20 Root Power Spectrum of the Spacecraft Attitude Error: *y*-Direction**



**Figure 23 Root Power Spectrum of the Test Mass 2 Suspension Force - *y***



**Figure 21 Root Power Spectrum of the Spacecraft Attitude Error: *z*-Direction**



**Figure 24 Root Power Spectrum of the Test Mass 2 Suspension Force - *z***